Outdoor Channel Modeling at D-Band Frequencies for Future Fixed Wireless Access Applications

Brecht De Beelde, Emmeric Tanghe, David Plets, and Wout Joseph

***Abstract*—Fixed wireless access networks at millimeter wave frequencies enable an alternative to fiber-optic installations for providing high-throughput internet connectivity. In this letter, we present outdoor channel measurements at D-band frequencies ranging from 120 GHz to 165 GHz, contributing to the design of future fixed wireless access networks. We measure angular path loss (PL) for both Line-of-Sight (LOS) and non-Line-of-Sight (NLOS) scenarios and calculate angular spread. We also measure building reflection loss for different angles and building facades. Directional LOS PL equals free-space PL, whereas omnidirectional PL is slightly lower. The angular spread of the LOS measurements is 19.7°. The omnidirectional NLOS PL model has a higher PL and the angular spread increases to 54.4°. Losses up to 11 dB should be taken into account for reflection on a fiber cement or building brick facade. and up to 15.6 dB and 18.5 dB for roughcast and stone bricks. Even though wireless communication via the direct path is preferred, reflected paths can enable high-throughput wireless communication if the direct path is obstructed.**

***Index Terms*—Fixed wireless access, D-band, outdoor, channel modeling, angular, path loss, reflection loss.**

I. Introduction

DURING the past decade, the need for broadband connectivity has increased. Not only do end-users require more data volumes and higher data rates, e.g., for video-on-demand streaming services, but also the data volumes of enterprises have risen. To enable broadband access, network operators are required to update their access networks, as data rates of current digital subscriber line (DSL) technology are generally limited to 100 Mbps [1]. Passive optical networks using fiber enable download rates up to 10 Gbps [2] but have a high installation cost [3]. Recent advancements in radio technology have enabled millimeter wave (mmWave) communication for frequencies up to 100 GHz [4], providing data rates up to 30 Gbps [5]. The large bandwidths that are available in the mmWave spectrum enable high-throughput wireless communication for applications such as fixed wireless access (FWA). In FWA applications, the last mile of the access network is replaced by wireless point-to-point links.

To realize reliable outdoor communication links for FWA and fifth-generation (5G) applications, outdoor channel models are created. Different path loss (PL) models exist. Single frequency floating-intercept (FI) and close-in (CI) PL models are presented in [4], [6]–[12]. A multi-frequency alpha-beta-gamma (ABG) model is presented in [12], [13]. In [6], a PL model is provided for FWA applications at sub-6 GHz frequencies, with frequency, distance, and antenna heights as model parameters. At higher frequencies, directional antennas are used to overcome the high free space PL (FSPL). Directional PL refers to the PL that is obtained from power measurements with a directional antenna, whereas omnidirectional PL refers to PL that is measured with an omnidirectional antenna. Outdoor measurements at 28 GHz using two directional horn antennas confirm that 1 Gbps downlink rates can be delivered for distances up to 100 m [7]. The probabilistic PL modeling approach in [8] shows that FI and CI PL models have similar results. In [9], directional and omnidirectional PL models are presented, based on outdoor measurements at 32 GHz using an omnidirectional transmit (TX) antenna and directional receiver (RX) antenna and for distances up to 141 m. Omnidirectional PL models at 28, 38, and 73 GHz are presented in [10]. In [11], the applicability of the 3GPP [12] and ITU-R [14] PL models at higher mmWave frequencies is discussed. A model for NLOS propagation over rooftops and along street canyons for frequencies up to 100 GHz is presented in [13].

In the D-band, ranging from 110 GHz to 170 GHz, even more bandwidth is available, and the lower atmospheric absorption loss compared to the 60 GHz band makes it appealing for future FWA and sixth-generation (6G) applications [15]. Current research on D-band channel modeling focuses on indoor propagation, e.g., for office environments [16], [17]. Indoor propagation, reflection, and penetration loss measurements at 140 GHz are presented in [18] for a broad set of materials. A comparison between the 28 GHz and 140 GHz channel models for a shopping mall environment confirms the fewer multipath components at 140 GHz, but the strongest paths show a high correlation [19]. Outdoor measurements at 142 GHz, with a distance of 15 m between the antennas, show excess losses ranging from 15 dB to 30 dB for reflected paths in a street canyon [20].

In this letter, we present angular path loss measurements for D-band frequencies in a university campus environment and derive wideband FI models and ABG models for LOS and NLOS scenarios. To the best of the authors' knowledge, this is the first time that angular PL measurements in an outdoor environment are presented for frequencies ranging from 120 GHz to 165 GHz and for distances up to 95 m. Furthermore, we present building reflection loss measurements for different incident angles and facades and connect the reflection loss measurements to the angular PL measurements.

In Section II, we present the measurement equipment and measurement scenarios. The channel modeling results follow in Section III, and Section IV concludes this letter.

B. De Beelde, E. Tanghe, D. Plets, and W. Joseph are with Ghent University/IMEC, Department of Information Technology, Ghent, Belgium, e-mail:Brecht.DeBeelde@UGent.be.

 https://doi.org/10.1109/LWC.2022.3202921

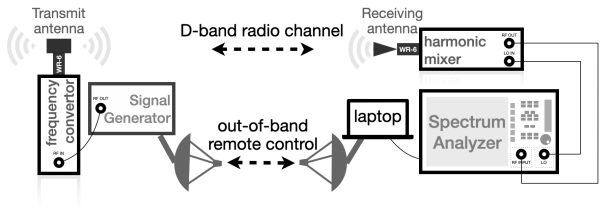

Fig. 1. Channel sounder architecture.

II. Methodology

A. Channel sounding architecture

The architecture of the channel sounder that is used for the measurements is presented in Fig. 1. The validation of the channel sounder is presented in [21]. A signal generator generates a continuous wave signal in the frequency range 9.13 GHz to 14.13 GHz, which is up-converted to the D-band using a frequency multiplier with multiplication factor 12. An omnidirectional vertically polarized antenna with a gain of 3 to 4 dBi, connected to the frequency multiplier via a WR-6 waveguide, is used as the transmitting (TX) antenna. The antenna has an azimuth beamwidth of 360° and an elevation half-power beamwidth (HPBW) of 45°. As receiving (RX) antenna, a directional horn antenna with a gain of 23 dBi is used. The horn antenna has a mid-band azimuth HPBW of 12° and an elevation HPBW of 8°. The horn antenna is connected to a harmonic mixer that down-converts the received D-band signal to an intermediate frequency ranging from 5 MHz to 3 GHz, using a local oscillator (LO) signal ranging from 9.13 to 14.13 GHz. The mixer has a frequency-dependent conversion loss ranging from 20 dB to 30 dB, with a measurement uncertainty of 1.5 dB. The power of the received signal is measured via a spectrum analyzer with a noise figure of 3 dB and a displayed average noise level of -151 dBm when using a resolution bandwidth of 100 Hz. The cable for connecting the spectrum analyzer's LO port to the mixer has a loss of 1.7 dB in the LO frequency range. Using a transmit power of 6 dBm, the maximum measurable PL of the channel sounder is 150 dB.

The TX antenna is mounted on a tripod, which allows height adjustments and horizontal leveling. The RX antenna is placed on a rotational platform which allows horizontal leveling and fine-tuned height adjustments, as well as rotating the antenna in steps of 12°. The signal generator and spectrum analyzer are connected to a laptop that is used to control the frequency on both devices. This allows performing a manual frequency sweep from 120 GHz to 165 GHz in steps of 1 GHz. At the spectrum analyzer, a frequency span of 1 MHz around the center frequency is used with 501 frequency points and averaging factor 4. The resolution bandwidth is fixed at 100 Hz, which results in a sweep time duration of 19 ms. The conversion loss data of the harmonic mixer is taken into account. Measured PL is found by subtracting the received power from the transmit power, and adding antenna gains. Antenna gain variations and cable losses are corrected via calibration [22].

B. Measurement environment and scenarios

We performed measurements along multiple tracks, categorized into LOS and NLOS. For each measurement track, the TX antenna location is fixed, and there are multiple RX antenna locations. At every RX antenna location, an azimuthal angular scan is performed by physically rotating the RX antenna over 360° in steps of 12°, which corresponds to the antenna's HPBW in the azimuth plane. From the angular power measurements, we gather PL angular profiles (PLAP), displaying PL as a function of the RX angle of arrival (AoA). The results of the measured PLAP are correlated to the measurement environments. From the PLAP, we calculate omnidirectional PL via (1), with $\mathrm{P_{TX}}$ the transmit power in dBm, $\mathrm{G_{TX}}$ and $\mathrm{G_{RX}}$ the gains in dBi of the TX and RX antennas, respectively, and PL(θ) the PL in dB with θ ranging from -180° to 180° in steps of 12°.

$$\begin{aligned}\mathrm{PL} =& \mathrm{P_{TX}} + \mathrm{G_{TX}} + \mathrm{G_{RX}} \\ &- 10\log_{10}\left(\sum_{\theta} 10^{(\mathrm{P_{TX}}+\mathrm{G_{TX}}+\mathrm{G_{RX}}-\mathrm{PL}(\theta))/10}\right)\end{aligned} \tag{1}$$

The summation over 30 azimuthal angles results in omnidirectional PL as the angular step size equals the HPBW of the RX antenna.

The measured PL values of all tracks are averaged over all frequencies and fitted to the wideband FI model from (2), with d the distance in meters, PL_0 the reference PL in dB at 1 m, n the PL exponent, and χ_σ the shadow fading term in dB, based on a zero-mean normal distribution with standard deviation σ.

$$\mathrm{PL_{FI}}(d) = \mathrm{PL}_0 + 10n\log_{10}(d) + \chi_\sigma \tag{2}$$

In addition to a wideband FI model, we also fit all PL values to the multi-frequency ABG model from (3), with intercept α, PL exponent β, frequency dependence γ, distance d in meters and frequency f in GHz.

$$\mathrm{PL_{ABG}}(d,f) = \alpha + 10\beta\log_{10}(d) + 10\gamma\log_{10}\left(\frac{f}{140\ \mathrm{GHz}}\right) + \chi_\sigma \tag{3}$$

We calculate root-mean-square (RMS) angular spread (AS) via (4), with θ the angle of arrival in degrees, ranging from -180° to 180°, and $\mathrm{P_{RX}}(\theta)$ the corresponding received power in Watt.

$$\mathrm{AS_{AoA}} = \sqrt{\frac{\sum_\theta \mathrm{P_{RX}}(\theta)\cdot\theta^2}{\sum_\theta \mathrm{P_{RX}}(\theta)} - \left(\frac{\sum_\theta \mathrm{P_{RX}}(\theta)\cdot\theta}{\sum_\theta \mathrm{P_{RX}}(\theta)}\right)^2} \tag{4}$$

1) Line-of-Sight path loss: We perform LOS measurements along seven tracks, with antenna separations ranging from 2 m to 95 m, and using an antenna height of 1.2 m, which allows better leveling of the antennas compared to higher heights. The TX antenna location is fixed, and the directional RX antenna is moved away from the TX antenna along a straight line in steps of 1 m. Every 1 m, a directional PL measurement is performed, i.e., with the RX antenna pointing towards the TX antenna. Every 10 m, a full angular scan is performed.

2) Non-Line-of-Sight path loss: Six NLOS tracks are measured for which the direct path between the two antennas is obstructed, and for which a reflected path exists. The obstructed (direct) path distances range from 9 to 26 m.

Fig. 2. Measurement setup for fiber cement reflection measurements with a 45° incident angle.

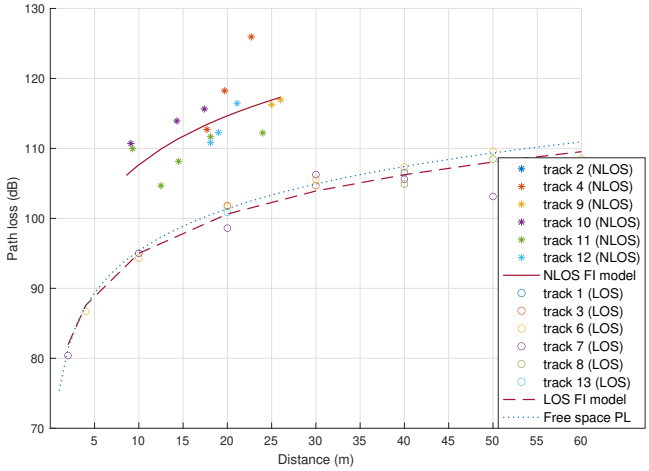

Fig. 3. Measured omnidirectional Line-of-Sight and non-Line-of-Sight wideband path loss in dB as a function of distance.

TABLE I
FITTED PARAMETERS OF WIDEBAND FI MODEL.

scenario	PL_0	n	RMSE
Directional LOS	75.9 dB	1.84	1.13 dB
Omnidirectional LOS	71.0 dB	1.89	1.35 dB
Omnidirectional NLOS	78.9 dB	2.46	5.48 dB

3) Building and car reflection: In addition to LOS and NLOS measurements, we consider car reflection and building reflection for different types of building facades, i.e., coated glass, fiber cement, stone bricks, stone building blocks, and roughcast. For each surface, both TX and RX antennas are placed at a distance of 3 m to the reflection point, and the directional RX antenna points to the reflection point, as can be seen in the measurement setup shown in Fig. 2. The incident angles, with respect to a line normal to the surface, range from 0° to 75° in steps of 15°. We measure specular reflection by using identical TX and RX angles and subtracting FSPL for a distance of 6 m from the measured PL.

III. RESULTS

A. Line-of-Sight and non-Line-of-Sight path loss models

Table I shows the fitted parameters of the wideband FI PL model from (2), as well as the root mean squared error (RMSE) between the PL samples and the fitted models. Omnidirectional wideband PL for both LOS and NLOS scenarios is shown in Fig. 3. For directional LOS, the reference PL at 1 m, i.e., PL_0, equals FSPL. In the omnidirectional LOS model, PL_0 decreases due to the received power in the multipath components. For the omnidirectional NLOS model, both PL_0 and the PL exponent increase, as well as the RMSE due to a higher spread between measured PL samples. Apart from a higher reference PL, the results are similar to the PL models at 32 GHz from [9]. In [10], omnidirectional PL exponents ranging from 1.8 to 2.1 are reported for LOS scenarios and ranging from 2.4 to 3.5 for NLOS scenarios at frequencies up to 73 GHz.

The directional LOS PL measurements have a limited frequency correlation, which is confirmed by analyzing the ABG model from (3). The intercept α equals 75.2 dB which is close to the fitted PL_0 from the FI model. The PL exponent β is 1.92 and γ is 1.25. For omnidirectional LOS measurements, α is 70.1 dB, β is 1.98, γ is 2.78, and the RMSE is 2.86 dB. For the NLOS measurements, the intercept α of 82.3 dB is higher than the PL_0 of the FI model, β equals 2.11, and γ equals 3.74. The RMSE of 4.86 dB is slightly lower than for the wideband FI model. For both LOS and NLOS scenarios, the coefficient of determination ([23]) of the FI and ABG models is similar, i.e., both models can equally explain the variance of path loss based on the model variables, and the wideband FI model is effective in predicting PL.

Figure 4 presents the PLAP for frequency 140 GHz at different distances for LOS and NLOS tracks. It shows measured PL as a function of AoA, after removing all PL values that were within 6 dB of the spectrum analyzer's noise floor. AoA 0° corresponds to the direct path between TX and RX antenna. In Fig. 4a, we see a strong LOS component for AoA 0°, as well as some reflections that are more apparent for the smaller distances. Figure 4b shows that for the NLOS scenarios, received power is much more distributed over the different multipath components, i.e., there are multiple reflected NLOS paths with similar PL values, compared to the single dominant path for the LOS scenarios.

Figure 5 connects the results from the PLAP to the environmental characteristics for two tracks. For LOS track 1, where the RX antenna moves parallel to the building, there is a reflection for AoA 50°, which corresponds to the reflection on the coated glass window of the building facade. The significant reflections for negative AoA correspond to reflections on the trees next to the building. NLOS track 9 has an attenuated obstructed LOS path with a PL of 132 PL for a distance of 26 m, which is 30 dB higher than FSPL for a similar distance. The measured PL for AoA 132° is 125.5 dB, which corresponds to a building reflection. In general, the excess losses of the reflected paths are higher than in a street canyon, due to a longer path length and smaller incident angles.

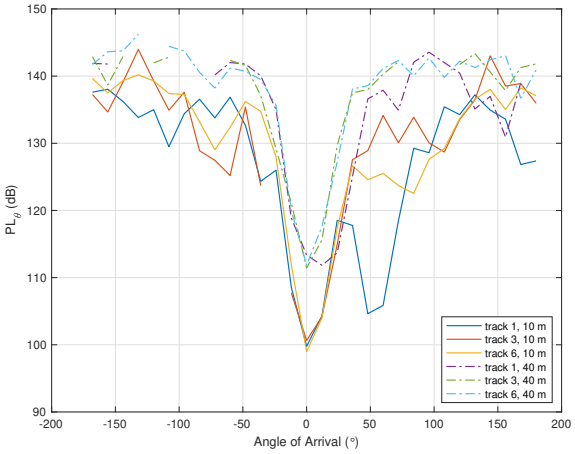

(a) Line-of-Sight track

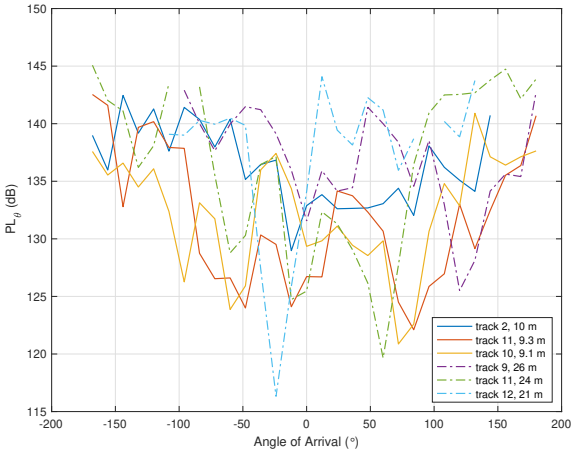

(b) non-Line-of-Sight track

Fig. 4. Angular path loss profiles at 140 GHz for different measurement tracks and different distances.

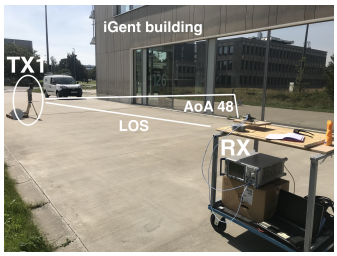

(a) LOS track 1, distance 10 m

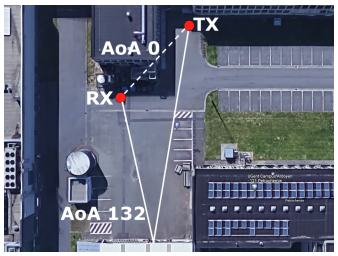

(b) NLOS track 9, distance 26 m

Fig. 5. Angular analysis based on environmental characteristics.

The mean angular spread, calculated via (4), increases from 19.7° for the LOS tracks to 54.4° for the NLOS tracks. This is in line with the angular spread values at D-band frequencies for indoor environments, with distances up to 10 m, reported in [24]. These results confirm the lower angular spread at mmWave frequencies compared to lower frequencies, which was also reported in [25]. The angular spread at mmWave

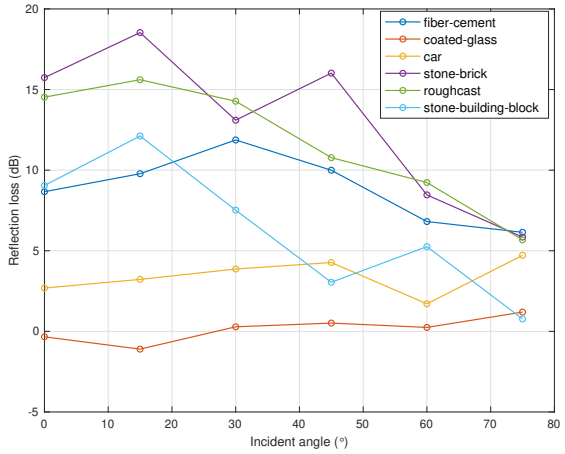

Fig. 6. Specular reflection loss as a function of incident angle for different surfaces for frequency 140 GHz.

frequencies is higher than at THz frequencies. In [26], angular spread at 300 GHz is modeled via raytracing for an indoor environment, with values around 10° to 20° for LOS scenarios and values around 20° for NLOS scenarios. In line with existing models, angular spread decreases with increasing frequency [27].

B. Building and object reflection

In the design of FWA networks, it is crucial to assess whether a reflected NLOS link provides a valid communication path. From the angular profiles shown in Sect. III-A, we already concluded that strong reflections can be present. To enable path loss prediction of a reflected path, we measure reflection loss for several building facades, as well as a car, for different incident angles. Adding this reflection loss to the path loss corresponding to the total path distance then gives the total path loss of the reflected path.

The measurement results for 140 GHz are summarized in Fig. 6. There is an expected trend of lower reflection losses for higher incident angles. Coated glass behaves as a perfect electrical conductor, with reflection losses that are within the measurement error of the system. This explains the low PL of the reflected path in track 1. Reflection on the metallic side of a car results in reflection losses ranging from 1.7 dB to 4.7 dB. The higher reflection loss for a car, compared to coated glass, can be explained by the curvature of the car, i.e., the field of incidence is not perpendicular to the reflecting surface. We also see that the stone brick facade has higher reflection losses compared to the wall made with building blocks. Even though the material characteristics are assumed to be similar, the mortar joints are more pronounced for the brick stones, resulting in more scattered energy. The fiber cement facade, which can be considered smooth even at D-band frequencies, has losses ranging from 6.1 dB to 11.9 dB. Roughcast, which has a higher granularity, has higher losses, from 15.6 dB for small incident angles to 5.7 dB for larger incident angles. The measured reflection loss for glass is lower compared to the

measurements presented in [18], whereas, the reflection loss for most facade materials is higher than the losses for materials used in indoor applications such as acrylic and wood that have smaller height variations compared to the building facades.

From the PLAP in Fig. 4b, we see a strong reflection for NLOS track 9 for AoA 132°. This can be related to a building reflection by analyzing the map of the environment, shown in Fig. 5b. The reflected path has a path length of 107 m, with a propagation loss of 116 dB. The incident angle is 12°, and the reflection loss for reflection on a fiber cement facade with an incident angle of 15° is 10 dB. Adding the reflection loss to the propagation loss results in a total PL of 126 dB which corresponds to the value seen in Fig. 4b.

IV. Conclusions

In this letter, we have presented outdoor channel measurements at D-band frequencies for future FWA applications. FWA applications are characterized by static propagation environments with antenna separations up to 100 m and antennas placed above ground level, to limit the influence of traffic and human activity. Our measurements confirm that, in the ideal case of an unobstructed LOS path, PL equals FSPL, and reflections can be significant. To estimate received power for the reflected NLOS paths, reflection measurements are performed for different facade types, as well as a car. If the direct path is obstructed, the reflected path can provide the high data rates that are required, as building reflection losses are lower than 15 dB for most building facades. Coated glass behaves like a perfect electrical conductor. Fitting wideband omnidirectional NLOS PL to an FI PL model shows that both reference PL and PL exponent increase compared to the wideband omnidirectional LOS PL model. The PL samples are also fitted to a multi-frequency ABG model that, for NLOS scenarios, has a slightly better performance compared to the wideband FI model, but the coefficient of determination does not improve significantly and the simpler FI model is effective in estimating PL. The analysis of the angular PL profile shows that multiple reflected NLOS paths contain comparable power, which can increase the link capacity using spatial diversity techniques. In future work, the PL models and reflection losses will be used for link budget calculations and network planning of future FWA networks.

Acknowledgment

This work was executed within the imec AAA D-band channel modeling research project (D-BARC).

References

[1] K. J. Kerpez and R. Kinney, "Integrated DSL test, analysis, and operations," *IEEE Transactions on Instrumentation and Measurement*, vol. 57, no. 4, pp. 770–780, 2008.

[2] D. Nesset, "PON roadmap [invited]," *Journal of Optical Communications and Networking*, vol. 9, no. 1, pp. A71–A76, 2017.

[3] N. Ioannou, D. Katsianis, and D. Varoutas, "Comparative techno-economic evaluation of lte fixed wireless access, fttdp g.fast and fttc vdsl network deployment for providing 30 mbps broadband services in rural areas," *Telecommunications Policy*, vol. 44, no. 3, p. 101875, 2020.

[4] I. A. Hemadeh, K. Satyanarayana, M. El-Hajjar, and L. Hanzo, "Millimeter-wave communications: Physical channel models, design considerations, antenna constructions, and link-budget," *IEEE Communications Surveys Tutorials*, vol. 20, no. 2, pp. 870–913, 2018.

[5] *IEEE 802.11ay-2021 - IEEE Standard for Information Technology–Telecommunications and Information Exchange between Systems Local and Metropolitan Area Networks–Specific Requirements Part 11: Wireless LAN Medium Access Control (MAC) and Physical Layer (PHY) Specifications Amendment 2: Enhanced Throughput for Operation in License-exempt Bands above 45 GHz*. IEEE Computer Society, 2021.

[6] Z. E. Khaled, W. Ajib, and H. Mcheick, "An accurate empirical path loss model for heterogeneous fixed wireless networks below 5.8 GHz frequencies," *IEEE Access*, vol. 8, pp. 182 755–182 775, 2020.

[7] J. Du, D. Chizhik, R. Feick, M. Rodríguez, G. Castro, and R. A. Valenzuela, "Suburban fixed wireless access channel measurements and models at 28 GHz for 90% outdoor coverage," *IEEE Transactions on Antennas and Propagation*, vol. 68, no. 1, pp. 411–420, 2020.

[8] M. K. Samimi, T. S. Rappaport, and G. R. MacCartney, "Probabilistic omnidirectional path loss models for millimeter-wave outdoor communications," *IEEE Wireless Communications Letters*, vol. 4, no. 4, pp. 357–360, 2015.

[9] X. Zhao, S. Li, Q. Wang, M. Wang, S. Sun, and W. Hong, "Channel measurements, modeling, simulation and validation at 32 GHz in outdoor microcells for 5G radio systems," *IEEE Access*, vol. 5, pp. 1062–1072, 2017.

[10] T. S. Rappaport, G. R. MacCartney, M. K. Samimi, and S. Sun, "Wideband millimeter-wave propagation measurements and channel models for future wireless communication system design," *IEEE Transactions on Communications*, vol. 63, no. 9, pp. 3029–3056, 2015.

[11] G. R. MacCartney and T. S. Rappaport, "Rural macrocell path loss models for millimeter wave wireless communications," *IEEE Journal on Selected Areas in Communications*, vol. 35, no. 7, pp. 1663–1677, 2017.

[12] 3GPP, "Technical specification group radio access network; channel model for frequency spectrum above 6 GHz (release 14)," 2016.

[13] ITU-R-P.1411-6, "Propagation data and prediction methods for the planning of short-range outdoor radiocommunication systems and radio local area networks in the frequency range 300 mhz to 100 ghz," International Telecommunication Union, Tech. Rep., 2012.

[14] M. Series, "Guidelines for evaluation of radio interface technologies for imt-advanced," *Report ITU*, vol. 638, pp. 1–72, 2009.

[15] J. Wells, "Faster than fiber: The future of multi-g/s wireless," *IEEE Microwave Magazine*, vol. 10, no. 3, pp. 104–112, 2009.

[16] B. De Beelde, E. Tanghe, C. Desset, A. Bourdoux, D. Plets, and W. Joseph, "Office room channel modeling and object attenuation at sub-THz frequencies," *Electronics*, vol. 10, no. 14, 2021.

[17] S. Ju, Y. Xing, O. Kanhere, and T. S. Rappaport, "Millimeter wave and sub-terahertz spatial statistical channel model for an indoor office building," *IEEE Journal on Selected Areas in Communications*, vol. 39, no. 6, pp. 1561–1575, 2021.

[18] B. De Beelde, D. Plets, C. Desset, E. Tanghe, A. Bourdoux, and W. Joseph, "Material characterization and radio channel modeling at D-band frequencies," *IEEE Access*, vol. 9, pp. 153 528–153 539, 2021.

[19] S. L. H. Nguyen, J. Järveläinen, A. Karttunen, K. Haneda, and J. Putkonen, "Comparing radio propagation channels between 28 and 140 GHz bands in a shopping mall," in *12th European Conference on Antennas and Propagation (EuCAP 2018)*, 2018, pp. 1–5.

[20] C. Larsson, B.-E. Olsson, S. Nguyen, and M. Johansson, "Propagation measurements comparing indoor and outdoor hotspot coverage at 28, 58, and 143 GHz," in *2022 16th European Conference on Antennas and Propagation (EuCAP)*, 2022, pp. 1–5.

[21] B. De Beelde, E. Tanghe, D. Plets, and W. Joseph, "Outdoor line-of-sight path loss modeling at 140 GHz," in *2022 16th European Conference on Antennas and Propagation (EuCAP)*, 2022, pp. 1–4.

[22] B. De Beelde, R. De Beelde, E. Tanghe, D. Plets, K. Verheyen, and W. Joseph, "Vegetation loss at D-band frequencies and new vegetation-dependent exponential decay model," *submitted to IEEE Transactions on Antennas and Propagation*, 2022.

[23] D. C. Montgomery, E. A. Peck, and G. G. Vining, *Introduction to Linear Regression Analysis (5th ed.)*. Wiley & Sons, 2012.

[24] L. Pometcu and R. D'Errico, "An indoor channel model for high data-rate communications in D-band," *IEEE Access*, vol. 8, pp. 9420–9433, 2020.

[25] J. M. Kelner, C. Ziółkowski, and B. Uljasz, "Comparison of angular spread for 6 and 60 GHz based on 3GPP standard," in *2018 22nd International Microwave and Radar Conference (MIKON)*, 2018, pp. 286–290.

[26] S. Priebe, M. Jacob, and T. Kürner, "Angular and rms delay spread modeling in view of THz indoor communication systems," *Radio Science*, vol. 49, no. 3, pp. 242–251, 2014.

[27] "TR 38.901: Study on channel model for frequencies from 0.5 to 100 GHz," 3rd Generation Partnership Project (3GPP), Tech. Rep., 2017.